Low spring index, large displacement Shape Memory Alloy (SMA) coil actuators for use in macro- and micro-systems

Invited Paper

Low Spring Index, Large Displacement Shape Memory Alloy (SMA) Coil Actuators for Use in Macro- and Micro-Systems

Brad Holschuh[a] and Dava Newman[b]

[a]Man-Vehicle Laboratory, Massachusetts Institute of Technology, 77 Massachusetts Avenue Room 37-219, Cambridge, MA, USA;
[b]Man-Vehicle Laboratory, Massachusetts Institute of Technology, 77 Massachusetts Avenue Room 33-307, Cambridge, MA, USA

ABSTRACT

Shape memory alloys (SMA) offer unique shape changing characteristics that can be exploited to produce low-mass, low-bulk, large-stroke actuators. We are investigating the use of low spring index (defined as the ratio of coil diameter to wire diameter) SMA coils for use as actuators in morphing aerospace systems. Specifically, we describe the development and characterization of minimum achievable spring index coiled actuators made from 0.3048 mm (0.012") diameter shape memory alloy (SMA) wire for integration in textile architectures for future compression space suit applications. Production and shape setting of the coiled actuators, as well as experimental test methods, are described. Force, length and voltage relationships for multiple coil actuators are reported and discussed. The actuators exhibit a highly linear ($R^2 > 0.99$) relationship between isometric blocking force and coil displacement, which is consistent with current SMA coil models; and SMA coil actuators demonstrate the ability to produce significant linear forces (i.e., greater than 8 N per coil) at strains up to 3x their initial (i.e., fully coiled) length. Discussions of both the potential use of these actuators in future compression space suit designs, and the broader viability of these actuators in both macro- and micro-systems, are presented.

Keywords: Shape memory alloys (SMAs), nickel titanium, active materials, active textiles, morphing systems, adaptive systems, MEMS actuators, coil actuators

1. INTRODUCTION

Active materials, sometimes referred to as artificial muscles, are a broad category of materials that respond in a repeatable manner when exposed to an applied stimulus.[1] Because of this ability, these materials have widespread engineering applications, including as embedded actuators for morphing systems.[1–10] Many types of materials exhibit shape changing properties, including (but not limited to) shape memory alloys (SMAs), shape memory polymers (SMPs), dielectric elastomer actuators (DEAs), and ionic polymer metal composites (IPMCs).[1] We are investigating the use of one of these materials, SMAs, as low mass, low bulk, large force and large displacement actuators. Our specific application focuses on the development of morphing wearable systems, but the actuators described in this paper have applications in any embedded active system. In the following sections, we present the design, modeling, manufacturing, and testing of strategically-designed, low spring index prototype SMA coil actuators, and discuss their use in both macro- and microelectromechanical- (MEMS) systems.

Shape memory alloys are a category of metal that exhibit thermally-induced shape recovery capabilities that stem from solid-state diffusionless phase transformations.[4] At low temperatures, SMAs assume a stable, face-centered tetragonal lattice martensite phase; once heated above a critical temperature, the material transforms to a high-temperature, body-centered cubic lattice austenite phase. This transformation triggers a repeatable change in shape (in the absence of external stress) that can be specifically tailored by annealing the material at high temperature in the desired memory shape.[4] The specific critical transformation temperatures of a given SMA can also be engineered, based on the alloys used and the annealing parameters selected.[4] The most common SMA, NiTi (referred to as Nitinol), has been used in everything from orthopedic implants to morphing aerospace structures.[4]

Send correspondence to B. Holschuh. E-mail: holschuh@mit.edu, Telephone: 1-701-367-9806

Reliability, Packaging, Testing, and Characterization of MOEMS/MEMS, Nanodevices, and Nanomaterials XIII, edited by Herbert R. Shea, Rajeshuni Ramesham, Proc. of SPIE Vol. 8975, 897505
 · doi: 10.1117/12.2044406

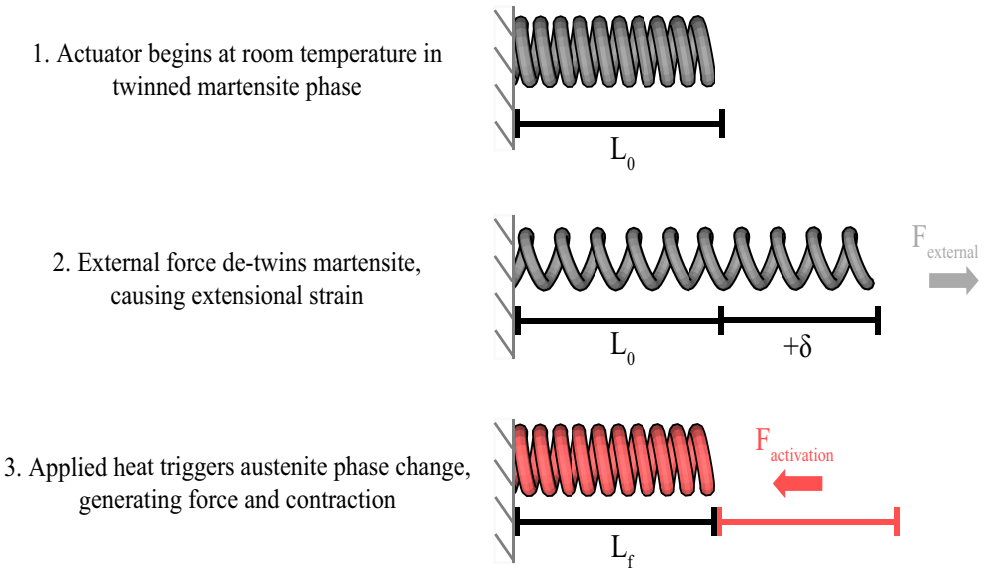

Figure 1. SMA coil actuator concept, depicted in three steps. Step 1: the actuator begins in the twinned martensite phase at low temperature. Step 2: an external force is applied to de-twin the actuator, stretching the spring and causing irrecoverable strain. Step 3: the actuator is heated above the critical temperature, resulting in a contraction and generated force. Once the actuator cools following step three, the cycle is reset and can begin again.

To best exploit the shape recovery characteristics of SMAs, actuators are frequently set as tightly packed springs. A shape-set spring is first stretched or deformed in the martensite phase (referred to as de-twinning the alloy), then heated above its critical temperature causing a contraction of the spring structure as the material changes phase.[4,7,9–14] As the actuator cools, it returns to the twinned martensite phase, resetting the actuator for the next de-twinning and actuation cycle. This cycle is depicted in Figure 1.

2. SMA COIL ACTUATOR DESIGN

The force F generated by a SMA spring actuator is dictated by a given set of geometric parameters: NiTi wire diameter d; spring diameter D, as measured by the midpoint between inner and outer diameters; number of active coils n; free spring length L_0, which is the total length of a fully-activated (i.e., austenite) actuator when unloaded; linear displacement δ; and shear modulus G. Actuator force follows Hooke's law, and can be expressed in simplified form as follows:[9,11,12]

$$F = k\delta = \left(\frac{Gd^4}{8D^3n}\right)\delta. \tag{1}$$

This model, which assumes complete austenite transformation, is a simplified version of those presented by An *et al.* and Seok *et al.*, but it is sufficient for our design purposes.[9,11] We can modify Eq. (1) to streamline actuator design by defining three non-dimensionalized parameters: packing density, η; actuator extensional strain, ϵ; and spring index, C.[15] We define packing density η as the ratio of the number of active coils n contained in the free spring length L_0 relative to the physical limit. This can also be defined as the ratio of the solid spring length L_S (i.e., the length of a spring that is wound as tightly as is physically possible) to the free spring length:

$$\eta = \frac{L_s}{L_0} = \frac{nd}{L_0}. \tag{2}$$

We define actuator extensional strain ϵ as the ratio of spring displacement δ to free spring length L_0:

$$\epsilon = \frac{\delta}{L_0}. \tag{3}$$

Spring index C is a universal spring parameter defined as the ratio of spring diameter D to wire diameter d, which is a measure of coil curvature d:[16–18]

$$C = \frac{D}{d}. \tag{4}$$

Substituting Eqs. (2), (3), and (4) into (1) provides us with the following form:

$$F = \frac{Gd^2}{8C^3\eta}\epsilon. \tag{5}$$

With Eq. (5), we can design actuators to meet specific performance requirements, which may include force targets, size limitations, manufacturing limitations, or desired lengths or extensional strains. For example, force is maximized by maximizing G, d, and ϵ, and by minimizing C and η. Physically speaking, maximum force is achieved when a SMA spring actuator is comprised of thick diameter wire wound to the tightest spring index, and is de-twinned to the mechanical limit with the lowest possible packing density. Such a design, however, requires tradeoffs in terms of actuator size and maximum actuator stroke length (i.e., longer stroke lengths can only be achieved when spring index is increased and packing density is increased, and large diameter SMA wire translates to large coil diameter, even with a minimized spring index). Alternatively, actuator design targets can be achieved by scaling the number of actuators used (if it is not possible to satisfy all constraints with a single actuator). However, increasing the number of actuators in a given system creates both a larger system footprint and greater power requirement. Therefore, specific consideration of each design variable must be given when engineering a system for a desired application.

We are specifically interested in creating morphing wearable structures using SMA coil actuators, to be used as constriction elements in a full body compression exploration space suit known as a mechanical counter-pressure (MCP) suit in partnership with NASA.[19–23] For this application, we prioritize maximum force generated (to create maximum counter-pressure) over other design variables, using the following criteria:

1. Maximize force by minimizing spring index C. A physical limit to the sharpness of curvature of a spring actuator exists, below which the material experiences structural damage.[16–18] We select actuators that match this minimum ($C = 3$).

2. Maximize force by selecting large d, within reason for a wearable system. While actuator force scales with the square of wire diameter (meaning that a maximum wire thickness should be used if force is to be purely maximized), this cannot be simply maximized due to design constraints associated with wearable garments (e.g., overly-thick actuators will encumber the wearer). Commercial NiTi wire is available as thin as $d = 25$ μm, and as thick as $d = 510$ μm*. We select reasonably large SMA wire diameters ($d = 305$ μm) to balance this tradeoff.

3. Enable large extensional strains ϵ by selecting high packing densities η. In addition to large active forces, MCP compression suits require significant active stroke lengths to accommodate donning and doffing prior to active compression. These requirements cannot both be maximized, in terms of selecting appropriate η and ϵ values (i.e., increased force calls for minimizing η, while increased stroke length calls for maximizing η because doing so increases maximum ϵ). Consequently, we select maximum η for a fixed C to provide as much extensional strain margin as possible.[15]

Prototype coil actuators with $C = 3$ have been shown to be mechanically limited to extensional strains approximately ≤ 3.[15] Because force varies with extensional strain, and extensional strain decreases as a coil actuator contracts, the initial pulling force will vary from the steady state pulling force (unless the actuator is fully blocked, resulting in no activation stroke and therefore no change in extensional strain). Using conservative estimates for material and actuation parameters ($G = 25$ GPa, $\eta = 0.9$, $\epsilon_i = 3$, and $\epsilon_f = 0.5$, representing an

*http://www.dynalloy.com/index.php

activation stroke length of 250% of the free length L_0) and the aforementioned design decisions (d = 305 μm, C = 3), we predict a single low spring index NiTi SMA actuator will produce the following initial (F_i) and steady state (F_{ss}) forces, assuming complete austenite transformation:[11]

$$F_i = \frac{(25 \cdot 10^9 \text{ Pa})(305 \cdot 10^{-6} \text{ m})^2}{8(3)^3(0.9)}(3) = 35.89 \text{ N}; \tag{6}$$

$$F_{ss} = \frac{(25 \cdot 10^9 \text{ Pa})(305 \cdot 10^{-6} \text{ m})^2}{8(3)^3(0.9)}(0.5) = 5.98 \text{ N}. \tag{7}$$

These values are based on an actuator comprised of commercially available SMA diameter wire that is slightly larger than average in terms of wire thickness (producing an actuator with an outer diameter of 1.22 mm). As previously stated, upper and lower bounds of SMA wire diameter available from Dynalloy, Inc., are 510 μm and 25 μm, respectively. Actuators with a fixed spring index (C = 3) made from these actuators would have outer diameters of 2.04 mm and 0.1 mm, respectively. Using the same parameter set as used in Eqs. (6) and (7), we predict initial and steady state activation forces for the full range of these commercially available SMA wire diameters (results shown in Figure 2). Force increases with the square of wire diameter and is linearly multiplied by ϵ (from 0.24-99.56 N at maximum ϵ, and from 0.04-16.59 N at an estimated steady state ϵ, assuming complete austenite transformation), and actuator outer diameter scales linearly with wire diameter (from 0.10-2.03 mm). These relations provide system designers with considerable freedom in designing actuators for a specific application, from micrometer-scale to millimeter-scale (and beyond). These freedoms in design will only increase as the number of actuators increase and constraints, such as minimum spring index, are relaxed.

3. COIL MANUFACTURING FOR MORPHING WEARABLE SYSTEMS

The method used to produce our prototype, low spring index NiTi coil actuators was adapted from Kim *et al.* and Seok *et al.*, and is depicted in Figure 3a.[9,12] To create the low-spring index structure prior to annealing, 305 μm NiTi Flexinol muscle wire [sourced from Dynalloy, Inc.] is wound around a 635 μm stainless steel core (producing a spring with C = 3.08) at room temperature (i.e., in the martensite phase). Winding is achieved by hanging the steel core from a variable speed DC motor, and the core is tensioned by a hanging weight attached via a low-friction bearing. The core rotates under tension as the motor spins; the SMA wire is knotted on one end to the core, which induces wrapping as the core rotates. To produce a tightly packed actuator (i.e., to achieve the highest possible packing density η), downward tension is induced in the NiTi wire manually, and upward tension is provided by a custom designed packing bar at the point of winding. Actuators produced using this method achieve η = 0.89 ($\pm$ 0.02, at 95% confidence).[15]

After winding is completed, the actuator is clamped on both ends to preserve the tightly packed spring form, and the structure is annealed at 450°C for 10 minutes (then water quenched) to lock in the desired memory state. These annealing parameters were selected based on a study conducted by Seok *et al.*, which identified 450°C as an annealing temperature that balances de-twinning force (which we seek to minimize) and permanent plastic deformation after actuation (which we also seek to minimize).[9] Finished actuators, both twinned and de-twinned, are shown in Figure 3b.

This method is easily adapted for a wide range of actuator sizes: actuator length is controlled by the amount of time the core is allowed to rotate (which sets the amount of SMA wire that winds, and therefore the total length); spring index is controlled by the size of the steel core relative to the wire diameter; and actuator width is controlled by the combined core and wire diameters. Seok *et al.* produced actuators using this method that were 3x smaller than those produced in this research effort (400 μm outer diameter vs. 1.24 mm) with the same spring index (C = 3). We select actuators to fit the design criteria for a controllable MCP suit architecture (e.g., maximized force for a given upper form-factor limit), but these actuators can be both up- and down-scaled depending on the application, assuming proper manufacturing precision can be obtained.

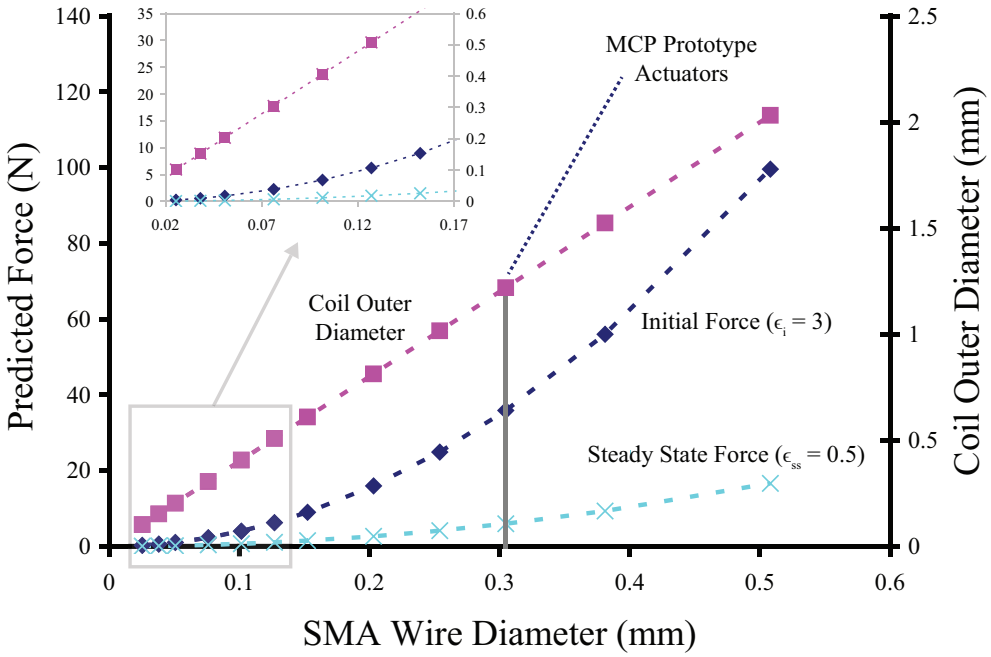

Figure 2. Predicted initial force (assuming $\epsilon = 3$), steady state force (assuming $\epsilon = 0.5$), and actuator outer diameter (assuming $C = 3.08$), for SMA spring actuators made from commercially available NiTi Flexinol wire (inset plot magnifies low diameter range). As wire diameter increases, actuator diameter linearly increases, and force increases with the square of wire diameter for a fixed ϵ. A wide range of forces and actuator diameters are possible given the choices in commercially available NiTi wire, providing considerable design freedom.

4. ACTUATOR PERFORMANCE

Multiple low spring index actuators were manufactured and tested to characterize their activation properties. Blocking force-extensional strain tests were conducted to validate the linear model presented in Eq. (5); voltage-force relationships were conducted to assess actuator controllability; several actuators were assembled in parallel to demonstrate the scalability of activation output; and activation-deactivation tests were conducted to assess the active force decay profile. These tests are described in detail in the following subsections.

4.1 Force-Extensional Strain Tests

A series of blocking force tests (i.e., tests that fix an actuator at a given extensional strain, then measure the steady state force as a voltage is applied) were conducted at varying extensional strains to assess the force generation properties and linearity of the prototype NiTi actuators. A variable height blocking force test stand was developed (depicted in Figure 3c) that measured activation forces through the use of a Futek LTH350 donut load cell [Futek Inc.]. An actuator was exposed to an 8V load for 60s at 3 different extensional strains ($\epsilon =$ 0.37, 1.00, and 1.73), and each test was repeated three times. The results of these tests are shown in Figure 4a. Each test run produced similar data: force increases quickly after the voltage is applied, and levels to steady state within 5s. Greater variability in the activation force was recorded at higher extensional strains (likely attributable to non-uniform heating and activation as the actuator is stretched to its limit). Force was found to be highly linear ($R^2 > 0.99$) across the extensional strains tested, validating the force displacement model (equation (5)). The highest average force measured was 8.94 N at $\epsilon = 1.73$, corresponding to a shear modulus $G = 10.80$ GPa, according to Eq. (5). This modulus value (which is lower than that reported by An *et al.*) is likely attributable to both the annealing parameters we selected as well as the alloy selection (i.e., using treated Flexinol wire vs. as-drawn Nitinol).[10,11]

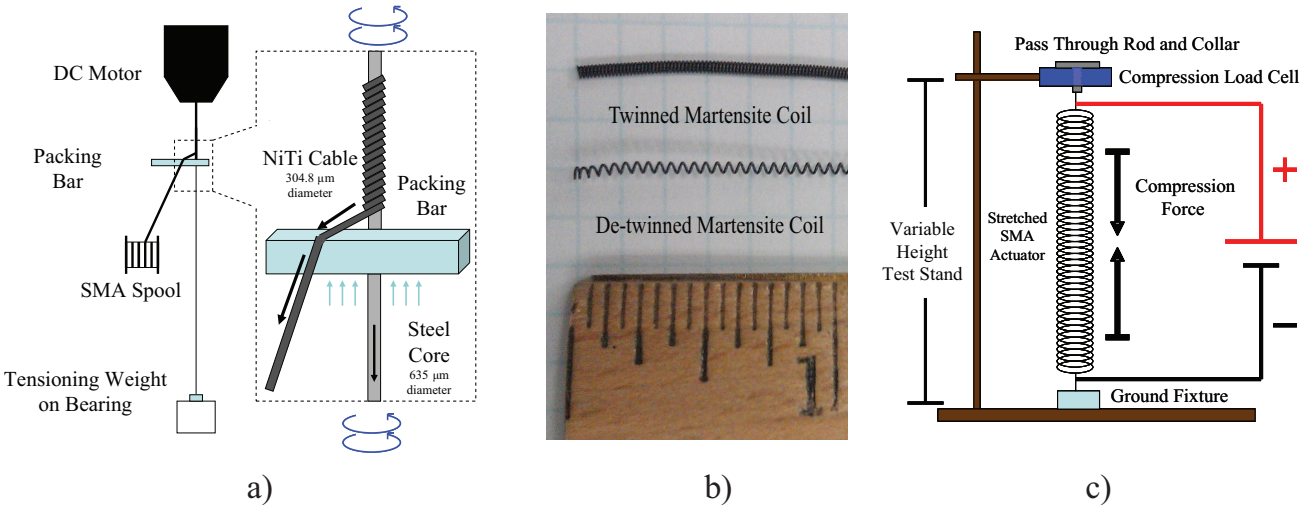

Figure 3. A (left): winding method to produce low spring index NiTi coil actuators, adapted from Kim *et al.* and Seok *et al.*[9,12] A stainless steel core is hung from a variable speed DC motor and attached to a weight via a bearing system. One end of the NiTi wire is fixed to the steel core, and as the steel core spins the NiTi wire wraps around the core. Tight packing is achieved through the use of a packing bar and by keeping the SMA wire under high tension. B (center): prototype SMA actuators (spring index $C = 3.08$, OD = 1.24 mm), shown in the twinned and de-twinned states. C (right): isometric blocking force test stand setup.

4.2 Force-Voltage Tests

A second test was conducted to assess the force-voltage behavior of a prototype actuator at a fixed extensional strain. The same isometric test stand was used, and an actuator was held at a fixed extensional strain ($\epsilon = 1.00$) and exposed to increasing voltages (from 0-10 V at 2 V increments, 2 minutes per voltage). The results of this test are shown in Figure 4b. At low voltages, no active force is measured, as the applied voltage does not generate sufficient Joule heating to cross the critical activation temperature (which, for 305 μm Flexinol wire, is listed to be 70°C). For all voltages $\geq$ 4 V, progressively increasing activation forces are measured as voltage is increased, indicating that the phase transformation of the actuator extends over a wide temperature range due to stress-induced reverse transformation (which follows the Clausius-Clapeyron relation and is consistent with published literature).[4,10] At 8 V, the average force profile reaches a maximum, indicating that complete austenite activation has been achieved. For voltages $>$ 8 V, we measure a significant loss of force (decaying to nearly zero). This is a result of overheating the actuator to the point that the memory state begins to reset (i.e., the actuator is effectively re-annealed at 10 V due to excessive Joule heating, causing a loss of memory and therefore a loss of active force). This behavior is significant from a design perspective for two reasons: first, force targets can be met either by directly altering the physical characteristics of an actuator to perfectly match the target (then heating the actuator to achieve full austenite transformation), or by over-designing the actuator and controlling the voltage such that only partial activation (and therefore, only partial active forces) are produced; second, system designers must avoid overheating the actuators, as this can lead to actuator shape memory loss and therefore a drastic loss in active force.

4.3 Performance of Multiple Actuators in Parallel

Four identical actuators were assembled in parallel to assess the force-voltage and power consumption relationships at a fixed extensional strain ($\epsilon = 1.36$). A circuit was assembled that connected the actuators in two parallel branches (with two actuators in each branch) connected in series with one another. Increasing voltages (from 2-5 V) were applied for 60s each, and both force and power consumption were measured. The results of this test are shown in Figure 4c. Again, force increases as voltage increases (along with power consumption), with the actuators reaching an average force of 24.75 N at 5 V (4.55 W). This corresponds to an average force of 6.57 N per actuator. Comparing this performance to the extensional strain tests in Figure 4a, we expect an actuator at 8 V and $\epsilon = 1.36$ to produce 7.90 N (based on interpolating the linear data). At considerably lower power (5 V vs.

8 V, which was conservatively selected based on temperature limitations in the support structure) we see 20.2% lower force, indicating that the parallel actuator setup could produce significantly higher forces than measured if greater voltage were to be applied. This test demonstrates the viability of linking multiple actuators in parallel to produce greater forces (at the cost of greater power requirements) with equivalent activation simplicity.

4.4 Actuation Decay Tests

A final test was conducted to assess the decay in activation force as the applied voltage is removed. The same four-actuator setup was tested at 5 V and a fixed extensional strain ($\epsilon = 1.36$), just as was done in the previous test. The test duration was 120s: at 10s, voltage was applied; at 80s the voltage was turned off; and force was measured for the full test duration (i.e., both during activation and deactivation). The results of this test are shown in Figure 4d. We see consistency in the activation data when compared to the previous test (overlaid on the plot for comparison), and we see significantly slower decay in force as the voltage is removed when compared to the equivalent force profile upon activation (i.e., actuators reach steady state force approximately 10s after activation, but when deactivated the force does not completely decay even after 30s). This is significant from a design perspective: activation and deactivation occur on different timescales, which needs to be accounted for when designing control systems using SMA actuators; and the time constants for activation and deactivation are large (on the order of 10s of seconds for these actuators, though this depends on actuator geometry, applied power, and wire diameter), meaning that systems requiring fast or dynamic responses may be poorly suited for SMA coil actuators.

5. DISCUSSION

Low spring index SMA actuators with these operating characteristics have use in a variety of systems, across several length scales. First, we summarize our modeling and experimental findings as follows, then we discuss potential macro- and MEMS-scale applications:

1. SMA actuators, which are known to have extremely high work density among active materials, typically do not produce large stoke lengths during activation when used in bulk, wire, or thin-film architectures (i.e., active strains are typically $\leq 8\%$).[1,24] SMA coil actuators, however, can produce stroke lengths $> 200\%$ when activated, while still producing large forces.

2. Minimum achievable spring index actuators ($C = 3$) produce the largest forces for a given coil outer diameter or SMA wire diameter. Actuators developed in this effort produced forces ≤ 8.94 N and achieved extensional strains $\epsilon \leq 3$. Their response is highly linear, and they are easily actuated through an applied voltage/current.

3. It is possible to produce minimum achievable spring index actuators using simple manufacturing techniques, and this method has repeatably produced actuators with outer diameters between 400-1200 μm.[9,15]

4. Commercially available SMA wire from Dynalloy, Inc., ranges in diameter from 25-510 μm, which would produce coil actuators with outer diameters 0.1-2.04 mm given a fixed minimum spring index. These actuators could theoretically produce individual forces up to 99.56 N depending on geometry, modulus, and extensional strain, and system performance will scale with the number of actuators used (providing several degrees of freedom in actuator design to meet application requirements).

5. Due to their dependence on thermal activation, SMA coil actuators have low frequency responses, and are poorly suited for systems that require dynamic, high frequency activation.[25] However, their frequency response does improve as SMA wire diameter (and therefore coil outer diameter) decreases, as the ratio of SMA surface area to volume increases, increasing convective heat transfer that results in faster cycling.[26] In fact, thermal-based MEMS actuators are the only category of actuators that demonstrate improvements in frequency response over their macro-scale equivalents.[26]

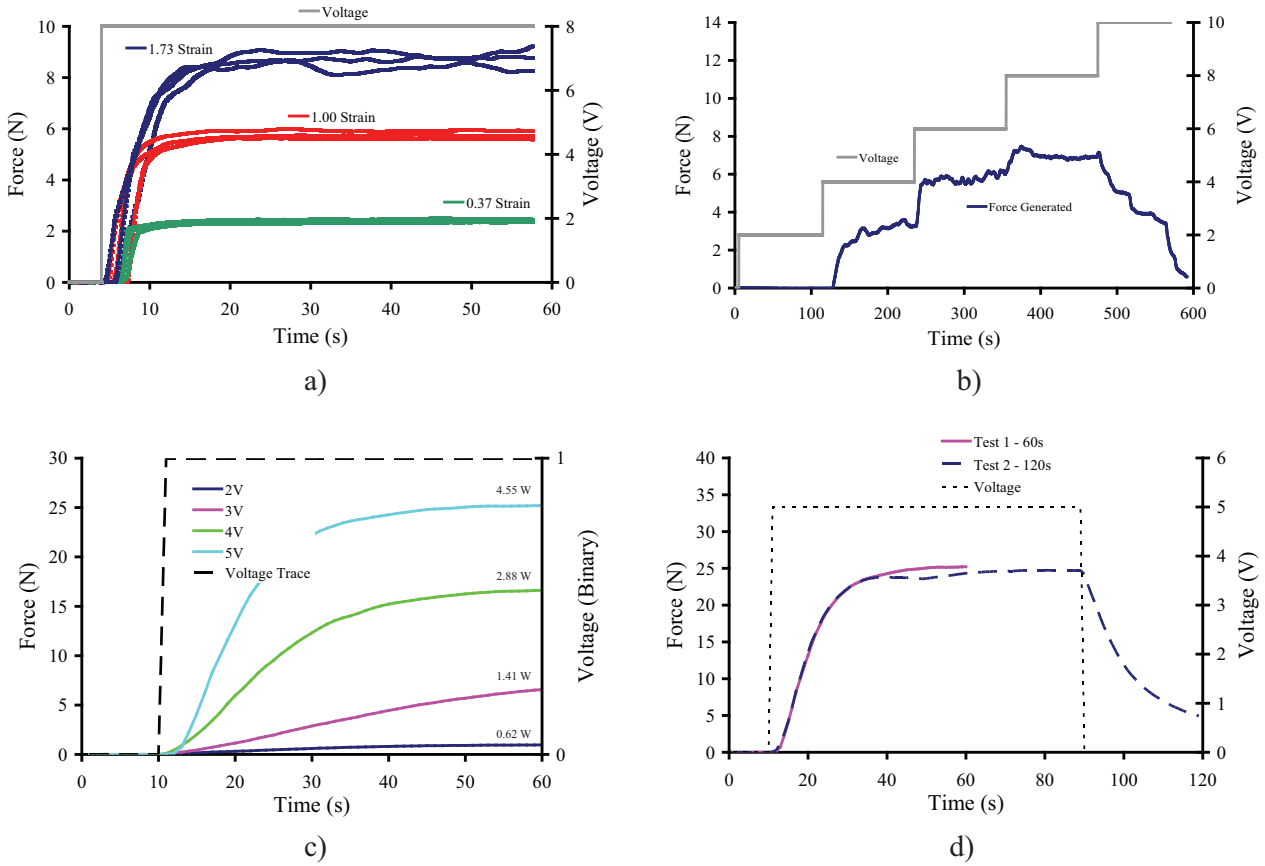

Figure 4. A (upper left): isometric blocking force data for a single actuator at three extensional strains. Force was found to vary linearly with extensional strain ($R^2 > 0.99$), as predicted by the force-displacement model, with the highest average force (8.94 N) measured at $\epsilon = 1.73$. B (upper right): force-voltage relationship for a fixed extensional strain ($\epsilon = 1.00$). Force increases as voltage increases (indicating a progressive austenite transformation), with maximum force occurring at complete austenite transformation (in this test this occurs at 8 V). Once voltage is increased beyond this point, significant losses in force are measured as the actuator is overheated and the memory state is reset. C (lower left): force-voltage-power relationship for four parallel actuators held at a fixed extensional strain ($\epsilon = 1.36$). Force increases with voltage and power, and is consistent with previous tests, demonstrating actuator scalability. D (lower right): Activation and deactivation force comparison. Time constants for activation and deactivation vary (i.e., actuators reach steady state active force in approximately 10s, whereas they do not fully deactivate after 30s of cooling).

6. Aside from low frequency response, the other limiting factor in SMA coil actuators is the fact that their activation is only one-way (i.e., the actuator must be deformed, or de-twinned, in the martensite state in order to produce a change in shape during phase transformation)[24,25,27,28]. Their use as actuators is therefore optimized in settings where a restoring or bias force is expected (or can be induced) at the beginning or end of each cycle.

7. In a blocking force setting, SMA actuators exhibit an extended voltage-force dependence (up to a maximum voltage, above which a loss in memory is observed as the actuator overheats and locally re-anneals). Consequently, blocking force configurations provide opportunities for increased activation resolution (as opposed to a typical, binary shape change response that occurs in the absence of blocking).[26]

8. SMA coil actuator cycle life is affected by the active strain induced per cycle - repeated small activation strokes result in lower cyclic deterioration than repeated large activation strokes.[1,24] Engineers must consider cycle life requirements when designing actuators for a given architecture, as blocking force config-

urations that prevent large activation strokes will demonstrate more stable cyclic actuator performance.

5.1 Macro-systems using SMAs

Macro-scale SMA coil actuators have widespread engineering applications,[1,2,4,5,7–14,16,29–34] particularly in the aerospace industry. Their low-bulk profile, high force and large active strains make SMA coil actuators particularly well suited for embedded aeronautics systems (like morphing wing structures, SMA "Smart Spar" systems, or propulsion system improvements like the SAMPSON program[4]) as well as space applications (like actuators for deployable and maneuverable solar panels, planetary robotic sensing and actuation systems, or even aids to prevent astronaut orthostatic intolerance).[35] As previously discussed, the primary motivation for this research effort is the development of wearable actuators for use in high-mobility MCP planetary exploration suits. The low profile, low bulk, high force and large displacement capabilities of low spring index coil actuators are perfectly suited for integration in a wearable garment, particularly one designed to constrict the wearer upon activation (as is the case in an MCP suit). Analysis of low spring index coil actuators as pressure-producing agents suggests that tourniquets comprised of a series of 1.2 mm outer diameter actuators (themselves comprised of 305 μm diameter NiTi Flexinol wire) can produce as much as 61.9 kPa active counter-pressure on a wearer's thigh at extensional strains $\epsilon = 0.5$ (for reference, the design specification for an MCP suit is 29.6 kPa).[15] A first-generation (and far from optimized) prototype tourniquet developed in-house based on this concept produced 4.9 kPa pressure production when activated. A refined prototype design is currently under development.[15] Active compression garments comprised of SMA coil actuators would vastly improve performance over traditional compression garments, which typically take the form of either static elastic garments (that are difficult to don and doff) or pneumatic bladders (that are bulky and require dedicated access to compressed air or fluid).[36–38]

5.2 Micro-systems using SMAs

MEMS architectures can also benefit significantly from the use of embedded low spring index SMA coil actuators. Previous studies examining SMAs as miniature linear actuators have concluded that spring-shaped actuators optimize mechanical performance for a given geometrical constraint (which is critical for micro-systems where space is at a premium),[28] and our analysis further identifies low spring index geometries as being the best spring design for maximum force generation. Typical MEMS applications that require significant actuation (e.g., micro-grippers, micro-valves, micro-pumps, tactile displays, and medical devices like micro-endoscopes) could produce larger forces using low spring index SMA coil micro-actuators than with any other traditional MEMS actuator (e.g., electrostatic actuators like Comb drives and Scratch drives, or piezoelectric or magnetic actuators) while exhibiting active displacements up to 3x their starting length.[26] Compared specifically to both electromagnetic and piezoelectric MEMS actuators, micrometer-scale low spring index SMA actuators excel in terms of both active force (10^{-2}-10^{-1} N vs. 10^{-7}-10^{-4} N and 10^{-5}-10^{-3} N, respectively) and achievable active displacement (10^{-3} m vs 10^{-5}-10^{-3} m and 10^{-7}-10^{-3} m, respectively).[26] Further, NiTi SMAs are biocompatible, which is particularly appealing for medical MEMS development.[4,25]

A challenge often reported when working with SMA actuators is the problem of mechanically mating the alloys to the surrounding structure while maintaining electrical conductivity, all without restricting the ability of the actuator to contract. This may be particularly challenging in MEMS system design, as actuators are miniaturized and assembled in tight proximity to other actuators or sensors. We have found particular success in this regard, on a macro-scale, by press-fitting and epoxying each end of an SMA coil actuator (or multiple actuators) between strategically designed (i.e., snap-together) 3D printed structures embedded with copper tape for electrical conductivity. These structures are then easily mated to both a base structure and to the object that is to be manipulated by the actuators. Acrylonitrile butadiene styrene (ABS) thermoplastic parts produced using a Stratasys Fortus 250mc printer [Stratasys, Ltd.] have performed without issue or degradation for our macro-scale prototyping, and the system offers a build layer thickness of 0.178 mm (with an achievable planar accuracy of $\pm$ 0.241 mm)[†]. Even greater accuracy can be achieved using more precise 3D printing equipment (e.g., the Stratasys Fortus 900mc printer offers an accuracy of $\pm$ 0.09 mm). Modern manufacturing techniques such as these, with sub-millimeter accuracy, may assist in the development of MEMS systems using low spring index SMA coil actuators.

[†]http://www.stratasys.com/3D-Printers/production-series/fortus-250mc

5.3 Summary

Low spring index SMA actuators combine large active forces (measured to be > 8 N for prototype actuators and predicted as high as 99.56 N using the largest commercially available SMA wire) with significant active extensional strains (up to $\epsilon = 3$ for actuators with the minimum achievable spring index $C = 3$). They are easily manufacturable using commercially available SMA wire, and can be scaled upward or downward to meet requirements for both macro- and micro-systems. A primary drawback of SMA actuators – low frequencies – improves as actuators are downscaled, and modern high-precision manufacturing methods may help to overcome traditional SMA system assembly issues, especially at the sub-millimeter scale. Taken collectively, these findings position SMA coil actuators as strong candidates for modern MEMS devices, particularly those that require large active forces and displacements.

ACKNOWLEDGMENTS

The authors would like to thank Lindsay Aitchison, Prof. Chris Schuh, Dr. Tricia Wilson, Dr. Leah Buechley, Edward Obropta, Dr. Chris Assad, Dr. Rajeshuni Ramesham, and Todd Billings for their contributions to this study. This work is supported in part by the National Aeronautics and Space Administration (NASA) Office of the Chief Technologist (OCT) under a Space Technology Research Fellowship (NSTRF), grant NNX11AM62H, and by the MIT Portugal Program (MPP).

REFERENCES

[1] Madden, J., Vandesteeg, N., Anquetil, P., Madden, P., Takshi, A., Pytel, R., Lafontaine, S., Wieringa, P., and Hunter, I., "Artificial muscle technology: physical principles and naval prospects," *IEEE J. Ocean. Eng.* **29 (3)**, 706–728 (2004).

[2] Lee, S.-K., Lee, S.-J., An, H.-J., Cha, S.-E., Chang, J. K., Kim, B. K., and Pak, J. J., "Biomedical applications of electroactive polymers and shape memory alloys," in [*Proc. SPIE*], **4695**, 17–31 (2002).

[3] Holschuh, B., Obropta, E., Buechley, L., and Newman, D., "Materials and textile architecture analyses for mechanical counter-pressure space suits using active materials," in [*AIAA Space 2012 Conf. Expo.*], AIAA, Pasadena, CA (2012).

[4] Lagoudas, D. C., [*Shape memory alloys: modeling and engineering applications*], Springer (2008).

[5] El Feninat, F., Laroche, G., Fiset, M., and Mantovani, D., "Shape memory materials for biomedical applications," *Adv. Eng. Mater.* **4 (3)**, 91–104 (2002).

[6] Haga, Y., Tanahashi, Y., and Esashi, M., "Small diameter active catheter using shape memory alloy," *Proc., 11th Annu. Int. Workshop Microelectromech. Syst.* , 419–424 (1998).

[7] Kim, B., Lee, M. G., Lee, Y. P., Kim, Y., and Lee, G., "An earthworm-like micro robot using shape memory alloy actuator," *Sens. Actuators A* **125**(2), 429–437 (2006).

[8] Pfeiffer, C., De Laurentis, K., and Mavroidis, C., "Shape memory alloy actuated robot prostheses: initial experiments," in [*1999 IEEE Int. Conf. Robot. Autom.*], 2385–2391 (1999).

[9] Seok, S., Onal, C. D., Cho, K.-J., Wood, R., Rus, D., and Kim, S., "Meshworm: A peristaltic soft robot with antagonistic nickel titanium coil actuators," *IEEE/ASME Trans. Mechatron.* **18 (5)**, 1485–1497 (2012).

[10] Stirling, L., Yu, C.-H., Miller, J., Hawkes, E., Wood, R., Goldfield, E., and Nagpal, R., "Applicability of shape memory alloy wire for an active, soft orthotic," *J. Mater. Eng. and Performance* **20 (4-5)**, 658–662 (2011).

[11] An, S. M., Ryu, J., Cho, M., and Cho, K. J., "Engineering design framework for a shape memory alloy coil spring actuator using a static two-state model," *Smart Mater. Struct.* **21 (5)** (2012).

[12] Kim, S., Hawkes, E., Cho, K., Jolda, M., Foley, J., and Wood, R., "Micro artificial muscle fiber using niti spring for soft robotics," in [*2009 IEEE/RSJ Int. Conf. Intell. Robots Syst.*], 2228–2234 (2009).

[13] Lee, H. J. and Lee, J. J., "Evaluation of the characteristics of a shape memory alloy spring actuator," *Smart Mater. Struct.* **9**(6), 817 (2000).

[14] Wang, Z., Zu, X., Feng, X., Zhu, S., Bao, J., and Wang, L., "Characteristics of two-way shape memory tini springs driven by electrical current," *Mater. and Des.* **25 (8)**, 699–703 (2004).

[15] Holschuh, B., Obropta, E., and Newman, D., "Low spring index niti coil actuators for use in active compression garments," *IEEE Transactions on Mechatronics* (Submitted November 4, 2013, for review.).
[16] Paredes, M., Sartor, M., and Masclet, C., "An optimization process for extension spring design," *Comput. Methods Appl. Mechanics and Eng.* **191**(8), 783–797 (2001).
[17] Budynas, R. G. and Nisbett, J. K., [*Shigley's mechanical engineering design*], McGraw-Hill New York (2008).
[18] Collins, J. A., Busby, H. R., and Staab, G. H., [*Mechanical design of machine elements and machines*], John Wiley and Sons (2009).
[19] Newman, D., Hoffman, J., Bethke, K., Carr, C., Jordan, N., Sim, L., Campos, N., Conlee, C., Smith, B., Wilcox, J., Trotti, G., and Mide-Technologies, "Astronaut bio-suit system for exploration class missions," *NIAC Phase II Final Rep.* (2005).
[20] Waldie, J., Tanaka, K., Tourbier, D., Webb, P., Jarvis, C., and Hargens, A., "Compression under a mechanical counter pressure space suit glove," *J. Grav. Physiol.* **9 (2)**, 93–98 (2002).
[21] Webb, P. and Annis, J., "The principle of the space activity suit," *NASA CR-973* (1967).
[22] Judnick, D., Newman, D., and Hoffman, J., "Modeling and testing of a mechanical counterpressure bio-suit system," in [*Int. Conf. Environmental Syst.*], 2007–01–3172 (2007).
[23] Tanaka, K., Danaher, P., Webb, P., and Hargens, A., "Mobility of the elastic counterpressure space suit glove," *Aviation, Space, Environ. Med.* **80 (10)**, 890–893 (2009).
[24] Kahn, H., Huff, M., and Heuer, A., "The tini shape-memory alloy and its applications for mems," *Journal of Micromechanics and Microengineering* **8**(3), 213 (1998).
[25] Bellouard, Y., "Shape memory alloys for microsystems: A review from a material research perspective," *Materials Science and Engineering: A* **481**, 582–589 (2008).
[26] Bell, D., Lu, T., Fleck, N., and Spearing, S., "Mems actuators and sensors: observations on their performance and selection for purpose," *Journal of Micromechanics and Microengineering* **15**(7), S153 (2005).
[27] Fu, Y., Du, H., Huang, W., Zhang, S., and Hu, M., "Tini-based thin films in mems applications: a review," *Sensors and Actuators A: Physical* **112**(2), 395–408 (2004).
[28] Nespoli, A., Besseghini, S., Pittaccio, S., Villa, E., and Viscuso, S., "The high potential of shape memory alloys in developing miniature mechanical devices: A review on shape memory alloy mini-actuators," *Sensors and Actuators A: Physical* **158**(1), 149–160 (2010).
[29] Yang, K. and Gu, C. L., "A novel robot hand with embedded shape memory alloy actuators," *J. Mech. Eng. Sci.* **216**, 737–745 (2002).
[30] Johnson, R., Padgett, J., Maragakis, M. E., DesRoches, R., and Saiidi, M. S., "Large scale testing of nitinol shape memory alloy devices for retrofitting of bridges," *Smart Mater. Struct.* **17**(3) (2008).
[31] Berzowska, J. and Coelho, M., "Kukkia and vilkas: Kinetic electronic garments," *9th IEEE Int. Symp. Wearable Comput.* (2005).
[32] Madill, D. R. and Wang, D., "Modeling and l2-stability of a shape memory alloy position control system," *IEEE Trans. Control Syst. Technol.* **6**(4), 473–481 (1998).
[33] Teh, Y. H., [*Fast, Accurate Force and Position Control of Shape Memory Alloy Actuators*], Australian National University (2008).
[34] Tadesse, Y., Thayer, N., and Priya, S., "Tailoring the response time of shape memory alloy wires through active cooling and pre-stress," *J. Intell. Mater. Syst. Struct.* **21**, 19–40 (2010).
[35] Platts, S. H., Tuxhorn, J. A., Ribeiro, L. C., Stenger, M. B., Lee, S., and Meck, J. V., "Compression garments as countermeasures to orthostatic intolerance," *Aviation, Space, Environ. Med.* **80**(5), 437–442 (2009).
[36] Diehm, C., Trampisch, H., Lange, S., and Schmidt, C., "Comparison of leg compression stocking and oral horse-chestnut seed extract therapy in patients with chronic venous insufficiency," *The Lancet* **347 (8997)**, 292–294 (1996).
[37] Brennan, M. J. and Miller, L. T., "Overview of treatment options and review of the current role and use of compression garments, intermittent pumps, and exercise in the management of lymphedema," *Cancer* **83**(S12B), 2821–2827 (1998).
[38] Doan, B., Kwon, Y.-H., Newton, R., Shim, J., Popper, E., Rogers, R., Bolt, L., Robertson, M., and Kraemer, W., "Evaluation of a lower-body compression garment," *J. Sports Sci.* **21**, 601–610 (2003).